JGR Atmospheres

RESEARCH ARTICLE
10.1029/2019JD032033

**Key Points:**
- OC correlated well with ozone during a photochemical pollution episode
- The OC atmospheric evolution was explained by a parameterization method
- The photochemical consumption of VOCs accounted for 67% of SOC formation

**Supporting Information:**
- Supporting Information S1

**Correspondence to:**
H. Wang,
wanghl@saes.sh.cn

**Citation:**
Wang, H., Wang, Q., Gao, Y., Zhou, M., Jing, S., Qiao, L., et al. (2020). Estimation of secondary organic aerosol formation during a photochemical smog episode in Shanghai, China. *Journal of Geophysical Research: Atmospheres*, *125*, e2019JD032033. https://doi.org/10.1029/2019JD032033

Received 11 NOV 2019
Accepted 13 MAR 2020
Accepted article online 22 MAR 2020

**Author Contributions:**
**Data curation:** Qian Wang, Min Zhou, Shengao Jing, Liping Qiao, Shengrong Lou, Shikang Tao, Yingjie Li
**Investigation:** Jingyu An
**Methodology:** Yaqin Gao, Cheng Huang, Jianmin Chen, Changhong Chen
**Resources:** Dandan Huang
**Writing – review & editing:** Bin Yuan, Joost A. de Gouw, Xuan Zhang



# Estimation of Secondary Organic Aerosol Formation During a Photochemical Smog Episode in Shanghai, China

**Hongli Wang[1], Qian Wang[1], Yaqin Gao[1], Min Zhou[1], Shengao Jing[1], Liping Qiao[1], Bin Yuan[2], Dandan Huang[1], Cheng Huang[1], Shengrong Lou[1], Rusha Yan[1], Joost A. de Gouw[3], Xuan Zhang[4], Jianmin Chen[5], Changhong Chen[1], Shikang Tao[1], Jingyu An[1], and Yingjie Li[1]**

[1]State Environmental Protection Key Laboratory of Formation and Prevention of Urban Air Pollution Complex, Shanghai Academy of Environmental Sciences, Shanghai, China, [2]Institute for Environmental and Climate Research, Jinan University, Guangzhou, China, [3]Department of Chemistry and Cooperative Institute for Research in Environmental Sciences, University of Colorado Boulder, Boulder, CO, USA, [4]Atmospheric Chemistry Observation and Modeling Laboratory (ACOM), National Center for Atmospheric Research (NCAR), Boulder, CO, USA, [5]Shanghai Key Laboratory of Atmospheric Particle Pollution and Prevention (LAP[3]), Department of Environmental Science and Engineering, Institute of Atmospheric Sciences, Fudan University, Shanghai, China

**Abstract** Secondary organic aerosols (SOA) are formed through diverse processes in the atmosphere, among which photochemical processing is one important pathway. SOA formation was studied based on one heavy photochemical smog episode in summer in Shanghai. During the pollution episode, ozone and organic carbon (OC) increased simultaneously with a strong positive correlation, which was complete opposite to the volatile organic compounds (VOCs) pattern but similar to that of VOC photochemical consumption. The OC evolution was explained well by a parameterization method based on the observation of OC and VOCs, and secondary OC (SOC) formation was derived, being comparable with the result based on elemental carbon (EC) tracer method. About 67% of SOC could be explained by the photochemical consumption of VOCs (mainly aromatics, ~93%) during the episode. The contribution of VOCs to SOC formation was also estimated from the available VOC emissions inventories, which was comparable with that based on VOCs observations in ambient. Some differences of VOC species contribution to SOC were found between the ambient observation-based and the emission-based results, and the contribution of C9 aromatics was underestimated in the emission inventory. This suggests that bias of speciation might exist in the current VOC emissions inventories. The present study highlights the importance of VOC oxidation for SOC formation in summer in Shanghai. More insights are needed to improve the accuracy of VOCs speciated emissions inventories.

## 1. Introduction

The formation of secondary organic aerosols (SOA) has been of great concern due to its large impacts on changing cloud properties and air quality (Hoyle et al., 2009). Generally, SOA are produced through the homogeneous (Claeys et al., 2004) and heterogeneous (Jang et al., 2002) reactions of volatile organic compounds (VOCs) and intermediate/semi-VOCs (Chan, et al., 2009; Robinson et al., 2007; Guo et al., 2020) as well as the aging of primary aerosols (Jimenez et al., 2009) in the atmosphere.

Although great strides have been made in the past decades, the estimation of SOA in the atmosphere is still highly uncertain (An et al., 2019; Ehn et al., 2014; Kanakidou et al., 2005; Shrivastava et al., 2017; Volkamer et al., 2006). It remains difficult to quantify the contribution of precursors in the ambient environment. Several field-based methods have been developed to estimate the amount of SOA, including the tracer-yield method (Guo et al., 2012; Kleindienst et al., 2007), the nonprimary organic carbon (OC) method (the receptor model) (Heo et al., 2015; Yuan et al., 2006; Zheng et al., 2002), the non–biomass burning water-soluble organic carbon method (Weber et al., 2007) and the elemental carbon (EC)-tracer method (or the OC/EC ratio method) [Cao et al., 2007; Song Guo et al., 2014; Turpin & Huntzicker, 1995; Zhang et al., 2008]. Among these methods, the receptor model can be used to apportion SOA in submicron particulate matter ($PM_{1.0}$) at a high time resolution from aerosol mass spectrometry (AMS) data (Hu et al., 2013;

Huang et al., 2012; Huang et al., 2014; Li et al., 2015; Sun et al., 2013; Zhang, 2005), while the tracer-yield method provides the only way of identifying precursors of SOA but with a low time resolution due to the complexity of tracer measurements.

In fact, both SOA and primary organic aerosols (POA) evolve simultaneously with the gaseous precursors in the atmosphere (Palm et al., 2018). The formation and loss of SOA interact with the aging and loss of POA and the gaseous precursors. The processing of organic aerosols (OA) and the potential gaseous precursors have been investigated in many field studies around the world (Ait-Helal et al., 2014; de Gouw et al., 2008; Gao et al., 2019; Hayes et al., 2013; Hayes et al., 2015; Jimenez et al., 2009; Kleinman et al., 2016; Koss et al., 2015; Sjostedt et al., 2011; Slowik, 2010; Weber et al., 2007; Yuan et al., 2013; Zhou et al., 2014). These studies have shown the amount of SOA to be several times that of the initial POA concentrations after a few hours of photochemical aging and have found a corresponding decrease in the concentrations of the gaseous precursors. These findings demonstrate the impact of the photochemistry of precursors on the formation of SOA.

Shanghai, the largest megacity in China with strong emissions of air pollutants (Fu et al., 2013; Li et al., 2014; Li et al., 2017), has suffered from severe pollution of fine particulate matter ($PM_{2.5}$) driven to a large extent by secondary formation (Huang et al., 2014; Wang et al., 2016) and increasing ozone concentration in the atmosphere (Li et al., 2019). Previous studies revealed SOA formation was enhanced by increasing atmospheric oxidizing capacity in north of China (Feng et al., 2019; Xu et al., 2017). This suggests the complex interaction and formation mechanisms of secondary pollutants. SOA and ozone share one kind of important precursors, while the impact of photochemical processing on the formation of SOA in Shanghai is unclear and the contribution of VOCs to SOA formation is ambiguous.

This study focuses on a pollution episode of $PM_{2.5}$ that occurred simultaneously with an $O_3$ episode in Shanghai in the summer of 2013. The evolution of OC and photochemical loss of VOCs was studied, and accordingly secondary OC (SOC) formation was derived, which was further compared with the estimation of SOC by the elemental carbon (EC) tracer method. The contribution of VOC oxidation to SOC formation was studied based on both the VOCs measurements in ambient and their emission inventory. Finally, the implication of SOC formation in Shanghai was discussed.

## 2. Experimental Methods

All measurements were conducted on the rooftop of a five-story building at a height of about 15 m from the ground in the Shanghai Academy of Environmental Sciences (SAES, 31.17°N, 121.43°E) from 2 to 12 August 2013, which is located in the southwest of the central urban area of Shanghai, China. A detailed description of the monitoring site is available from our previous studies (Qiao et al., 2014; Wang et al., 2013; Wang et al., 2016).

The mass concentration of $PM_{2.5}$ was measured with a resolution of 1 hr by an online particulate monitor (FH 62 C14 series, Thermo Fisher Scientific Inc.) using beta attenuation equipped with a verified $PM_{2.5}$ cyclone. The hourly concentrations of the carbonaceous species in $PM_{2.5}$ were measured by a semicontinuous OC/EC analyzer (model RT-4, Sunset Laboratory Inc.) equipped with an upstream parallel-plate organic denuder. The detailed principle and operation of these instruments have been described in detail elsewhere (Wang et al., 2015; Wang et al., 2016).

Fifty-five VOC species were continuously measured every 30 min by two online high-performance gas chromatograph with flame ionization detector (GC-FID) systems (Chromato-sud airmoVOC C2–C6 #5250308 and airmoVOC C6–C12 #2260308, France). The detection limits for VOC species range from several tens to hundreds pptv, as listed in supporting information Table S1. A detailed description of the measurements can be found in our previous study (Liu et al., 2019; Wang et al., 2013**)**.

The trace gases—nitrogen oxides ($NO_x$), carbon monoxide (CO), and ozone ($O_3$)—were routinely measured with a resolution of 1 min. All gas analyzers were calibrated using multipoint calibration. Meteorological parameters including wind speed, temperature, relative humidity, and solar radiation were also automeasured simultaneously during the pollution episode.

## 3. Results and Discussions

### 3.1. Overview of the Photochemical Pollution Episode

An episode of heavy photochemical smog occurred in Shanghai during the period of 2–12 August 2013, as shown in Figure S1. During this episode, the daily maximum of solar radiation reached 800 W/m$^2$ for a continuous period of over 7 days, and the daily peak temperatures were over 35 °C for a continuous period of over 11 days. The 24 hr back trajectories during the period were shown in Figure S2. As indicated, the air masses during the period were mostly from the south to southwest of Shanghai, which meant there were no significant variation of the meteorology. Meanwhile, the back trajectories during 5 to 11 August ($O_3$ pollution episode with the daily maximum 1 h-$O_3$ concentration exceeding 100 ppbv) were shorter than those of other days, suggesting the air mass was more stagnant during 5 to 11 August. The measured wind speed was 4.0 ± 1.5 m/s on average during the whole period, lower than the mean of the wind speed (4.5 m/s) in summer (June, July, and August) (Wang et al., 2016), and especially the wind speed during the $O_3$ pollution episode was as low as 3.5 ± 1.4 m/s. These meteorological conditions, combined with the relatively stagnant air mass and low humidity, hindered the dilution of air pollutants and induced the formation of photochemical smog. Consequently, for a continuous period between 5 and 11 August, the daily maximum 1 h-$O_3$ concentration exceeded Class II of China National Air Quality Standards (CNAAQS) for hourly average of 200 μg/m$^3$ (~100 ppbv). The increases in VOC and $NO_x$ concentrations played an important role in the high concentration of ozone during 5–11 August. The concentration of VOCs was as high as ~60 ppbv, doubling the annual average of ~27 ppbv (Wang et al., 2013**)**. The diurnal patterns of VOCs and $NO_x$ were completely opposite to that of $O_3$, demonstrating chemical losses of precursors contribute to the formation of $O_3$, as shown in Figures 1 and 2.

In the meantime, the $PM_{2.5}$ mass concentration reached high levels during the episode, averaging 48 μg/m$^3$ with hourly maximum of 94 μg/m$^3$. These values are significantly higher than those before and after the episode. The mass concentration of $PM_{2.5}$ was higher in daytime than nighttime, as shown in Figure 1, and showed a good agreement with $O_3$, with a correlation coefficient ($R$) of 0.65, as shown in Figure 3. According to a study in the western Yangtze River Delta region, these two pollutants are negatively correlated under low temperatures but positively correlated under high temperatures (Ding et al., 2013). This suggests the importance of the photochemical formation of $PM_{2.5}$ during a pollution episode.

OC accounted for 28.9% of $PM_{2.5}$, making it the most abundant component during the episode. If an organic matter OM/OC ratio of 1.8 is applied to estimate the mass of OA, the mass fraction of OA in $PM_{2.5}$ would be as high as 42%, which is comparable to the 48% reported in a previous study (Huang et al., 2014). There was a significant peak of the diurnal pattern of the OC/EC ratio during noontime, as shown in Figure 1. The correlation between OC and $O_3$ was even stronger than that between $O_3$ and $PM_{2.5}$, and the correlation coefficient ($R$) was 0.67, as shown in Figure 3. This suggests that the photochemical formation played more important roles in OC than in $PM_{2.5}$ during the episode.

### 3.2. SOC Formation From VOCs Oxidation ($SOC_{VOC}$)

#### 3.2.1. Photochemical Consumption of VOCs

As mentioned in section 3.1, the diurnal pattern of VOCs was completely opposite to that of $O_3$, and the concentration during nighttime was 18% higher than that of daytime (Table S1), suggesting the strong chemical loss of VOCs inducing the formation of photochemical pollution, as shown in Figure 2. VOC photochemical consumption was calculated in this section.

The photochemical consumption of VOCs can be described by equation 1 below, with the assumption that the oxidation of OH radicals dominates the loss of VOCs in the ambient environment. Generally, the photochemical age of the air masses could be described by the measured ratio of two VOC species with the similar emission sources but with different atmospheric reactivity and their measured uncertainties should relatively be low. Several ratios have been used to estimate the photochemical age, such as ethylbenzene to m,p-xylene, benzene to toluene, benzene to ethylbenzene, benzene to toluene, etc (de Gouw, 2005; Wang et al., 2013; Yuan et al., 2013). Correlations of benzene to toluene, benzene to ethylbenzene, and benzene to toluene with ozone were relatively bad, suggesting the sources of each couple of VOC species were not very similar in Shanghai. The photochemical age ($t$) of the air mass was estimated from the measured concentration ratios of ethylbenzene ($E$) to m,p-xylene ($X$) in this study, and the diurnal pattern of $E/X$ reflected

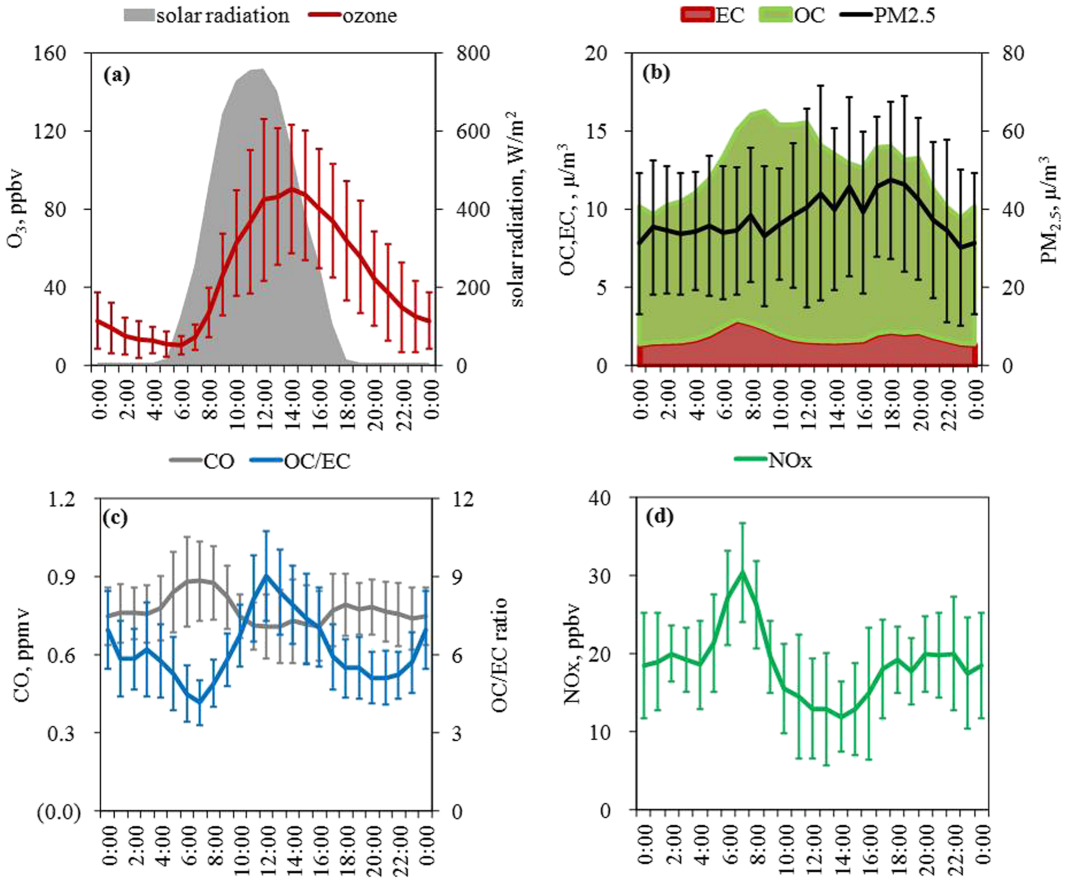


**Figure 1.** Diurnal variations of (a) ozone concentration and solar radiation, (b) $PM_{2.5}$, OC, and EC concentration, (c) CO concentration and the ratio of OC/EC, and (d) $NO_x$ concentration of the whole campaign.

the evolution of photochemistry in the present study as shown in Figure 2a, which has been proved to be suitable in Shanghai in our previous studies (Gao et al., 2019; Wang et al., 2013**)** according to equation 2 below.

$$VOC_{i,consumed} = VOC_{i,t} \times (\exp(k_i[OH]\Delta t) - 1) \quad (1)$$

$$\Delta t = \frac{1}{[OH](k_E - k_X)} \times \left(\ln\left\{\frac{[E]}{[X]}_{t=t_0}\right\} - \ln\left\{\frac{[E]}{[X]}\Big|_{t=T}\right\}\right) \quad (2)$$

Here, $VOC_{i,\ consumed}$ and $VOC_{i,\ t}$ are the consumption and measured concentrations of $VOC_i$, respectively. $k_i$ is the reaction rate constants of $VOC_i$ with OH radicals. $k_E$ ($7.0 \times 10^{-12}$ $cm^3$ $molecule^{-1}$ $s^{-1}$) and $k_X$ ($18.7 \times 10^{-12}$ $cm^3$ $molecule^{-1}$ $s^{-1}$) are the reaction rate constants of ethylbenzene ($E$) and m,p-xylenes ($X$) with OH radicals (Atkinson et al., 2006). [OH] is the concentration of OH radicals, which is not necessary for the calculation of $VOC_{i,\ consumed}$. $([E]/[X])_{t\ =\ t0}$ is the ratio between the initial mixing ratios of ethylbenzene and m,p-xylenes in the fresh emissions. Generally, there were several methods to get $([E]/[X])_{t\ =\ t0}$. (1) The first one is using the minimum of the measured ratios of $[E]/[X]$ in ambient but with enough data. (2) The second one is using the emission ratio of $[E]/[X]$ in the local sources. (3) The third one is using the average measured ratio of $[E]/[X]$ during the period with negligible photochemical processing, like 0:00–4:00. In the present study, considering the studied period was only 11 days, the $([E]/[X])_{t\ =\ t0}$ was using the lowest 10% value (0.6) of measured ratios of $[E]/[X]$ during summer (July, August, and September) in 2013, as shown in Figure S3. $([E]/[X])_{t\ =\ t}$ is the ratio of $[E]$ to $[X]$ at time $t$.

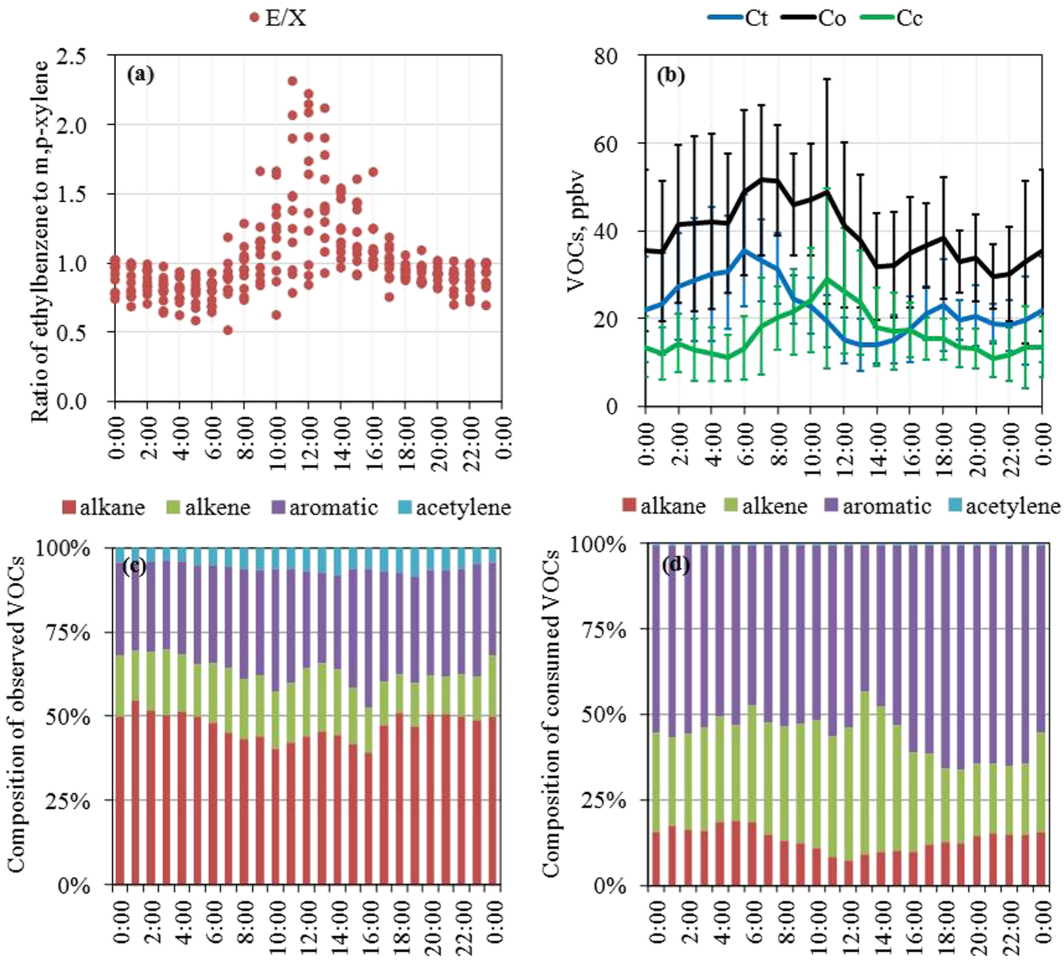


**Figure 2.** Diurnal pattern of (a) the ratio of ethylbenzene to m,p-xylene, (b) observed VOC concentrations (Ct) and chemical consumption concentrations (Cc), and chemical compositions of (c) measured and (d) consumed VOCs of the whole campaign.

Accordingly, the diurnal pattern of the concentration of VOC photochemical consumption (Cc) was shown in Figure 2b, with a peak at 11:00 with an average of 29.1 ± 20.1 ppbv, which was earlier than the time (at 14:00) with the lowest measured concentration (Ct). Based on equation 1, the photochemical loss of a given VOC was calculated using its observed concentration (Ct) and OH exposure ($[OH]\Delta t$) which was dependent

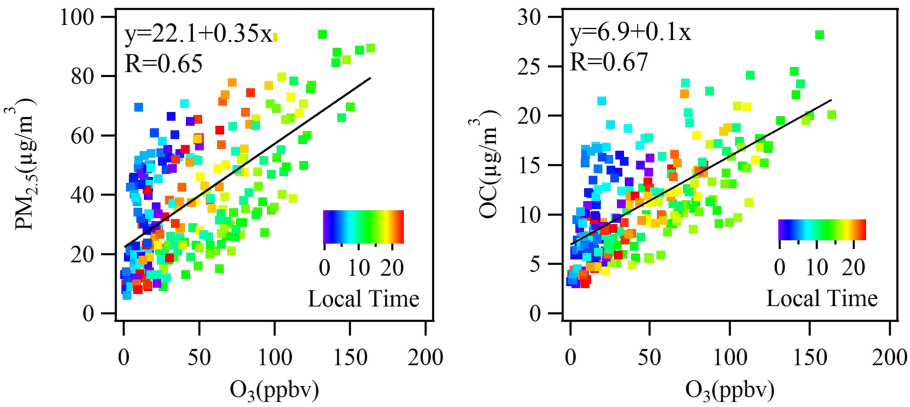


**Figure 3.** Scatterplots of (left) $PM_{2.5}$ and (right) OC with $O_3$ concentrations color-coded by local time.

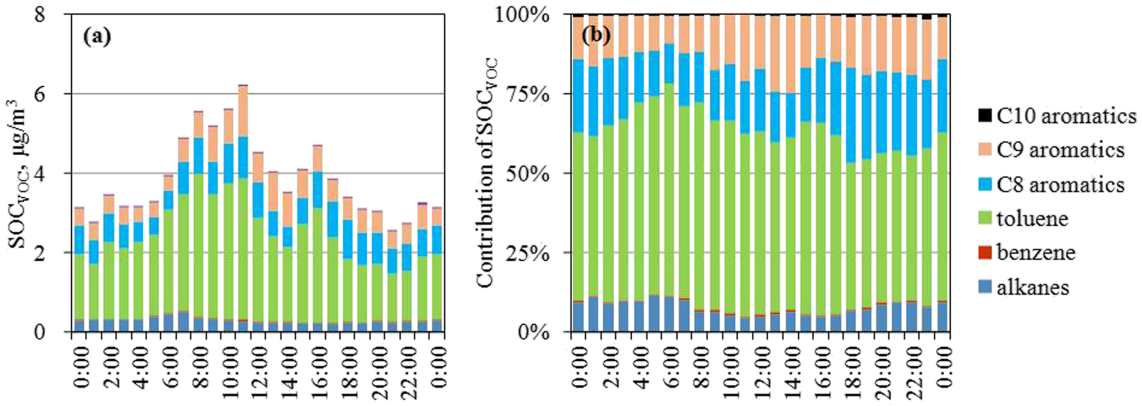


**Figure 4.** The average diurnal patterns of (a) $SOC_{VOC}$ and (b) its compositions.

on the observed ratio of ethylbenzene to m,p-xylene ($([E]/[X])_{t=t}$). It should be pointed out that there were some variations of the results, as shown in Figure 2b, which was probably due to the limited data in this study. On average, Cc was 17.2 ± 8.0 ppbv, slightly lower than Ct (22.7 ± 8.5 ppbv). For the initial concentration ($C_0$), its diurnal pattern had a peak in the early morning, which probably resulted from the traffic and human activities as well as the low mixing layer boundary. The lowest concentration of $C_0$ happened around 14:00, mainly due to the favorable diffusion conditions.

Meanwhile, the species compositions of consumed VOCs were highly different from those of measured VOCs, as shown in Figures 2c and 2d. Aromatics dominated the consumed VOCs, accounting for 55%, followed by alkene (32%) and alkane (12%). This means that aromatics and alkenes were more important precursors of photochemical processing due to their high reactivity than alkanes which dominated the measured VOCs.

### 3.2.2. $SOC_{VOC}$ Estimation

VOC photochemical consumption plays an important role in SOC formation in urban areas (eg., de Gouw et al., 2008; Ding et al., 2012; Emanuelsson et al., 2013; Gao et al., 2019; Guo et al., 2013; Spracklen et al., 2011). Based on the VOC photochemical consumption, the corresponding formation of SOC ($SOC_{VOC}$) was calculated using equation 3 as follows:

$$SOC_{VOC} = \mathrm{SOA}/1.8 = \left(\sum_i VOC_{i,\ consumed} \times Y_I\right)/1.8 \quad (3)$$

where $VOC_{i,\ consumed}$ is the consumption of $VOC_i$ as mentioned above; $Y_i$ is the SOA yield of $VOC_i$ oxidation which is determined from chamber studies; and the ratio of SOC to SOA is assumed to be 1.8.

The SOA yields have been published for most VOCs, and are 0 for small alkanes and alkenes, low for the higher (>C8) and cyclic alkanes, and the highest for aromatics (Seinfeld & Pandis, 2006). Previous studies showed that SOA yields of hydrocarbons heavily depended on $NO_x$ levels, mainly due to the competition reactions of $RO_2$ radical with NO and $HO_2$ radical (Ng et al., 2007). The most recent studies found that the dimerization of $RO_2$ radicals in the presence of autooxidation pathway at low $NO_x$ condition also play important role in the higher SOA yields (Praske et al., 2018; Schwantes et al., 2017). SOA yields of most aromatics under low-$NO_x$ conditions were significantly higher than those under high-$NO_x$ conditions (Ng et al., 2007). The average $NO_x$ concentration in the ambient was 2.9 ± 2.2 ppbv in this study, under which the chemistry occurring was consistent with that under high $NO_x$ conditions created in chamber studies. Chamber studies showed that SOA yields of aromatics under high-$NO_x$ conditions could be described using an empirical relationship based on gas-particle partitioning of two semivolatile products (Odum et al., 1996). The SOA yield from a given VOC was then used in the parameterization method and determined from ambient temperature ($T$ = 306.5 K in this study) and organic aerosol mass loading (OM = 19.0 μg m$^{-3}$ in this study). The vapor wall loss has been recognized to be underestimated largely, which resulted in the underestimation of chamber yields in previous studies. The vapor wall loss correction factors of SOA yields were

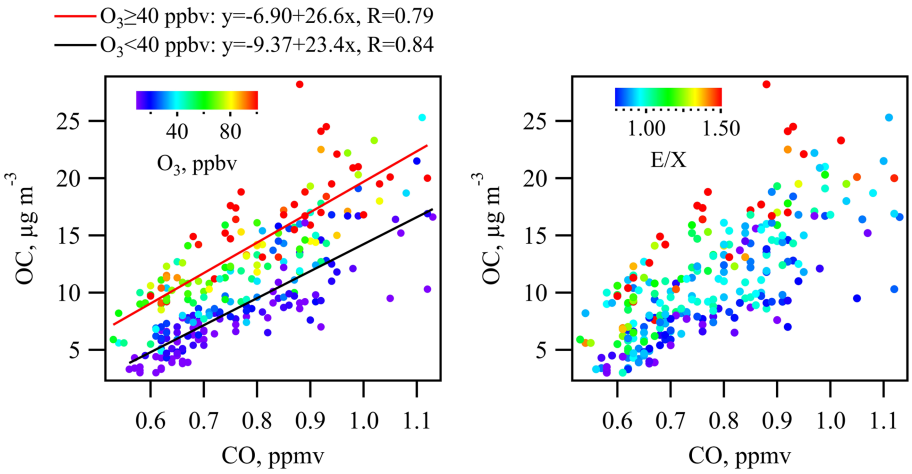


**Figure 5.** Scatterplots of OC and CO color-coded by $O_3$ (left) and the *E*/*X* ratio (right).

obtained from Zhang et al. (2014) in this study. Due to the lack of parameters in the two-product relationship and $NO_x$ dependence information for alkanes and cycloalkanes in the literature, SOA yields of these compounds are directly adapted from Lim and Ziemann (2009) and further corrected for vapor wall losses (Zhang et al., 2014). Sensitivity analysis of the selections of temperature and OC mass concentration to the yields calculation was tested using the hourly observed data and the impacts were found to be negligible (as shown in Figure S4). The calculated SOA yield of each VOC species were tabulated in Table S2.

$SOC_{VOC}$ determined from VOC oxidations was $3.9 \pm 1.0$ μg/m$^3$ on average during the whole period. The oxidation of aromatics dominated $SOC_{VOC}$ formation, accounting for 93% SOC, as shown in Figure 4. Specifically, toluene was the most important VOC precursor of $SOC_{VOC}$, accounting for 57% of SOCvoc, followed by C8 (19%) and C9 aromatics (16%). $SOC_{VOC}$ took up 35% of OC in $PM_{2.5}$ during the present episode. But how much did VOCs contribute to SOC during summer in Shanghai? To answer this question, SOC formed during the episode was estimated as described below.

### 3.3. SOC Estimation Via a Parameterization Method (SOC)

#### 3.3.1. SOC Estimation

Figure 5 showed scatterplots of OC versus CO color-coded by $O_3$ and the *E*/*X* ratio. As shown, OC correlated with CO well, and the correlation coefficients (*R*) were 0.84 ($O_3$ concentration <40 ppbv) and 0.79 ($O_3$ concentration ≥ 40 ppbv), respectively. The average ratio of OC to CO (~27 μg m$^{-3}$ ppmv$^{-1}$ for the data with $O_3$ concentration higher than 40 ppbv) was high during the periods with high concentrations of $O_3$ and high ratios of *E*/*X* indicating strong photochemistry, whereas this ratio (~23 μg m$^{-3}$ ppmv$^{-1}$ for the data with $O_3$ concentration lower than 40 ppbv) was low in the air mass with relatively low $O_3$ levels and low ratios of *E*/*X*. These observations further confirmed the large contribution of photochemical formation to OC.

A semiempirical relationship between OC/ΔCO and the photochemical age, Δ*t*, of urban plumes has been derived, which can explain a significant portion of the variation in the OC data (de Gouw, 2005; de Gouw et al., 2008; Yuan et al., 2013), where ΔCO was CO subtracted the background concentration to exclude the influences of emitted and transported OC. Accordingly, the measured concentrations of OC can be separated into primary emission, secondary formation and background concentration using equation 4 below:

$$\begin{aligned} OC &= ER_{OC} \times ([CO] - 0.6) \times \frac{\exp(L_{OC}\Delta t)}{\exp(-k_{OC}[OH]\Delta t)} \\ &+ ER_{precursor} \times Y_{OC} \times ([CO] - 0.6) \times \frac{P_{OC}}{L_{OC} - P_{OC}} \times \frac{\exp(-P_{OC}\Delta t) - \exp(-L_{OC}\Delta t)}{\exp(-k_{CO}[OH]\Delta t)} \\ &+ [bg] \end{aligned} \quad (4)$$

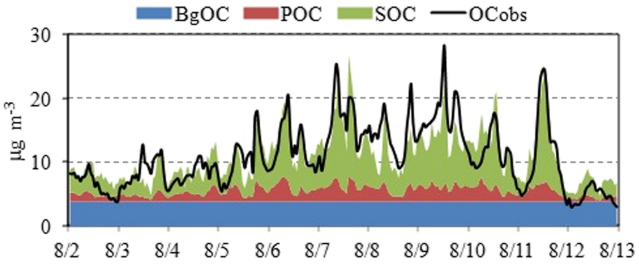


**Figure 6.** Time series of measured and simulated concentrations of OC during the episode. BgOC, POC, and SOC were the background concentration of OC, primary OC, and secondary OC; $OC_{obs}$ was the measured OC.

$ER_{OC}$ and $ER_{precursor}$ are emission ratios of OC and OC precursors to CO. $L_{OC}$ and $P_{OC}$ are the loss and formation rates of OC. $Y_{OC}$ is the yield of precursors that form OC. [CO] is the concentration of CO, with the background concentration of 0.6 ppmv (Figure S5), which is determined from the intercept in the scatterplot of CO with benzene by the method of DeCarlo et al. (2010). $k_{co}$ ($0.24 \times 10^{-12}$ $cm^3$ $molecule^{-1}$ $s^{-1}$) is the reaction rate constant of CO with OH radicals (Atkinson et al., *2006*). [bg] is the background concentration of OC (denoted by BgOC). The other parameters are the same as those in equation 1. [OH] is the average OH radical concentration ($1.7 \times 10^6$ molecule $cm^{-3}$) estimated from the empirical equation (Ehhalt & Rohrer, 2000). As shown in Figure S6, the average of the daily maximum concentration was about $6 \times 10^6$ molecule $cm^{-3}$, comparable with the only published result ($7 \times 10^6$ molecule $cm^{-3}$) in the summer of 2016 in Shanghai by Tan et al. (2019) from the observation-based model. Accordingly, the first item in equation 4 represents the primary emission of OC and its removal (denoted by POC). The second item represents the secondary formation of OC from the available precursors and its removal (denoted by SOC). The unknown parameters are $ER_{OC}$, $ER_{precursor} \times Y_{OC}$, $L_{OC}$, $P_{OC}$, and [bg].

In order to obtain more stable and reasonable fits, the initial settings of these five unknown parameters were given empirically. The lifetime of OC in the atmosphere fell in the range of 3–10 days (Koch, 2001; Millet et al., 2004), and correspondingly the value of $L_{OC}$ varied from $1.2 \times 10^{-6}$ to $3.9 \times 10^{-6}$ $s^{-1}$. The initial setting of production rate of OC ($P_{OC}$) was similar to that of $L_{OC}$. For the emission ratio of OC to CO ($ER_{OC}$), the result from the emission inventory of Shanghai was ~8 μg $m^{-3}$ $ppmv^{-1}$ (Fu et al., 2013), and the average measured ratio in the present study was 13.9 μg $m^{-3}$ $ppmv^{-1}$, and accordingly the initial setting of $ER_{OC}$ was 5 μg $m^{-3}$ $ppmv^{-1}$. The initial settings of the background concentration of OC (BgOC) and the product ($ER_{precursor} \times Y_{OC}$) of emission ratio of SOC precursor ($ER_{precursor}$) and its yield of SOC ($Y_{OC}$) referred to the results of Yuan et al. (2013) study.

After setting the initial values, the sensitivity of each parameter was tested to obtain reasonable fits. As shown in Figure S7, as OC lifetime varied from 4 days to 10 days, the fitted results of the other parameters were quite stable. To present the average results, the lifetime of OC was set as 6 days, and thus the uncertainty of OC loss rate ($L_{OC}$) was estimated as the standard variation with the OC lifetime ranging from 1 to 10 days. The uncertainties of other parameters were the standard variations of their variations with the change of OC lifetime. All the fitting results and uncertainties were summarized in Table S3.

The background concentration of OC was fitted to be 3.8 ± 0.4 μg $m^{-3}$, which was higher than that of 2.4 μg $m^{-3}$ on Changdao Island (Yuan et al., 2013). This was expected because the strong emissions around Shanghai city would have increased the background concentration of OC in Shanghai, whereas the emissions around Changdao Island would have been less strong seeing as it is located away from the city clusters. $ER_{OC}$ was determined to be 5.8 ± 0.5 μg $m^{-3}$ $ppmv^{-1}$, which was lower than the emission result (Fu et al., 2013). $ER_{precursor} \times Y_{OC}$ and $P_{OC}$ strongly coupled in the fit, and therefore hard to determine independently from each other.

The OC, POC, SOC, and BgOC were simulated based on the fitting parameters, as shown in Figure 6. On average, the correlation efficient ($R^2$) between measured ($OC_{obs}$) and simulated ($OC_{sim}$) concentrations was 0.723, as shown in Figure S9, and the average ratio between $OC_{sim}$ and $OC_{obs}$ was 1.1 ± 0.3. Accordingly, the fractions of POC and SOC in total OC were 12% and 49%, respectively.

### 3.3.2. OC Evolution Along With the Photochemical Age

According to the fitting results, the evolution of the simulated OC with the photochemical age was presented in Figure 7. Photochemical age was estimated by equation 2 above. [OH] is the average OH radical concentration ($1.7 \times 10^6$ molecule $cm^{-3}$) estimated from the empirical equation as mentioned above. As shown in Figure 7c, the primary emissions and the background concentrations were a significant fraction of OC in the first few hours. The secondary formation continued for about 3 days, after which OC was almost exclusively from secondary sources. Considering the estimated photochemical ages during the whole period in this study were lower than 20 hr, we fitted the data with photochemical age lower than 20 hr in Figure 7c by

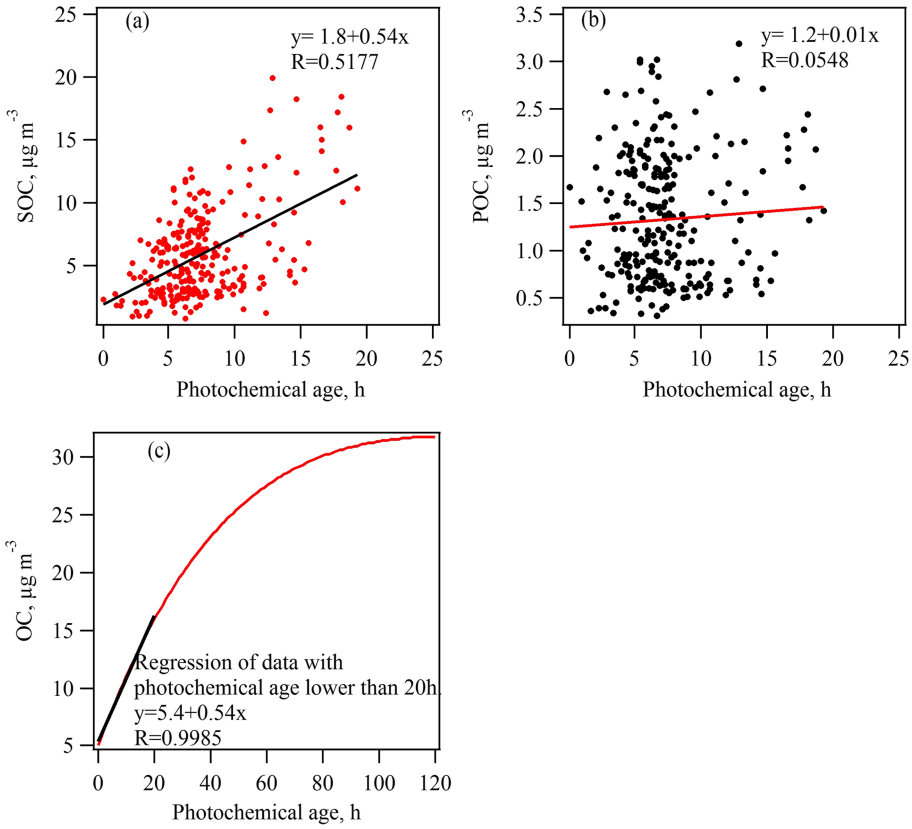


**Figure 7.** Scatterplots of the simulated (a) SOC and (b) POC with the photochemical age, and (c) the evolution of OC along with the photochemical age.

linear regression. The regression slope of OC versus photochemical age was 0.54 μg $m^{-3}$ $hr^{-1}$, which was comparable with the regression slope of the simulated SOC versus photochemical age in this study (as shown in Figure 7a). The simulated SOC increased as the photochemical age increased, and presented a good correlation with the photochemical age with the correlation coefficient (*R*) of 0.52. As expected, bad correlation of POC with the photochemical age was obtained.

### 3.4. SOC Estimation by EC Tracer Method (SOC′)

Elemental carbon (EC) has been widely used as a tracer to track the portion of co-emitted primary OC and, by extension, to estimate SOC from ambient observations of EC and OC (Turpin & Huntzicker, 1995). Key to this EC tracer method is to determine an appropriate OC/EC ratio that represents primary combustion emission sources (i.e., $(OC/EC)_{pri}$) at the observation site. The approaches include regressing OC against EC within a fixed percentile of the lowest OC/EC ratio data (usually 5–20%) or relying on a subset of samples with low photochemical activity and dominated by local emissions. Considering the limited measurement of the studied period, the present study estimated $(OC/EC)_{pri}$ (2.5) by the regression of OC and EC with the lowest 10% OC/EC ratios in August and September of 2013, as shown in Figure S10. Accordingly, SOC′ was estimated as 6.2 ± 3.4 μg/$m^3$.

### 3.5. Comparisons of SOC Calculated From Different Methods

Figure 8 compares the SOC calculated from the three methods mentioned above. As shown, SOC was 5.8 ± 3.6 μg/$m^3$ derived from the parameterization method in section 3.3 and 6.2 ± 3.4 μg/$m^3$ derived from the EC tracer method in section 3.4. These two values are comparable. SOCvoc (3.9 ± 1.0 μg/$m^3$) determined from the yield method in section 3.2 could explain 67.2% of total SOC, which was much higher than that (29%) of clean period in Shanghai in summer (Gao et al., 2019). It suggested that the photochemical oxidation of VOCs, especially aromatics, by OH radicals played important roles in SOC formation during the photochemical pollution episode in summer in Shanghai.

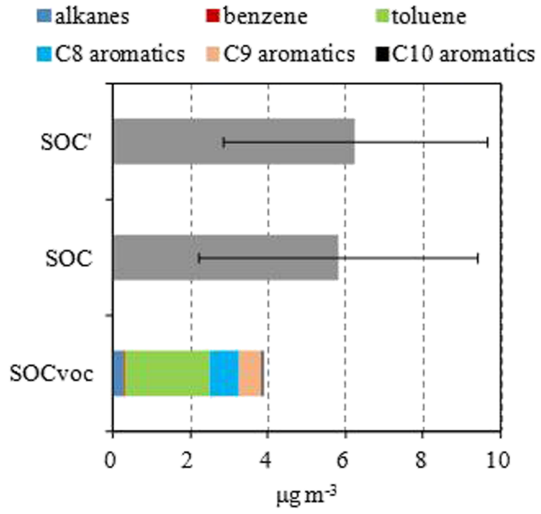


**Figure 8.** Comparisons of SOC calculated by different methods (the parameterization method for SOC; the EC tracer method for SOC′; the yield method for SOCvoc).

As shown, toluene SOA dominated SOCvoc. One important reason was due to the high SOA yield of toluene in the calculation. We corrected the yield of toluene SOA by a factor of 10 owing to vapor wall losses, but applied a wall-loss correction factor in the range of 1.16–1.25 for all the other alkanes and aromatic compounds (Gao et al., 2019; Zhang et al., 2014). There has been some evidence showing that toluene photochemistry that leads to SOA formation is unique. For example, Ng et al. (2007) reported that toluene yield is twice as much as xylenes. While benzene SOA yields are highest among the three, the degradation rate of benzene in the atmosphere is an order of magnitude slower than that of toluene so its contribution to SOA formation is considered much less important. Liu et al. (2016) measured the evaporation rates of particulate constituents of toluene SOA under all humidity ranges (0–50%) are a factor of 10 slower than those of SOA materials produced from xylenes.

### 3.6. Comparisons With the Previous Studies

For comparison with the previous studies, the OC/ΔCO ratio is used to evaluate the contribution of SOC formation, where ΔCO is CO subtracted the background concentration (0.6 ppmv in this study, as mentioned in section 3.3) to exclude the influences of emitted and transported OC (DeCarlo et al., 2010). With the formation of SOC, the OC/ΔCO ratio increased and thus the enhancement of the OC/ΔCO ratio, in other words Δ (OC/ΔCO), could represent the formation of SOC. Based on the diurnal pattern of OC/ΔCO ratio, the ratio rose from a minimum of 30.6 μg $m^{-3}$ $ppmv^{-1}$ at 6:00 to a maximum of 59.7 μg $m^{-3}$ $ppmv^{-1}$ at 12:00 on average in this study, with an increase of 28.5 μg $m^{-3}$ $ppmv^{-1}$. The Δ (OC/ΔCO) estimated in this study was higher than those of Beijing urban (7.8 μg $m^{-3}$ $ppmv^{-1}$) [*W* Hu et al., 2017], Guangzhou rural (20 μg $m^{-3}$ $ppmv^{-1}$) [W W Hu et al., 2012], and Changdao rural (10.4 μg $m^{-3}$ $ppmv^{-1}$) (Yuan et al., 2013) reported previously, as presented in Figure 9. It suggested, again, the strong photochemistry played very important roles in SOC formation during the ozone pollution episode in Shanghai.

The enhancement of OC/ΔCO ratio obtained above was higher than the average ratio of SOC/ΔCO (22.2 ± 5.7 μg $m^{-3}$ $ppmv^{-1}$) of the whole period, as shown in Figure 9. The average ratio of $SOC_{VOC}$/ΔCO was 14.9 ± 5.0 μg $m^{-3}$ $ppmv^{-1}$, accounting for 66.9% of SOC/ΔCO which was close to the proportion of $SOC_{VOC}$ in SOC mentioned in section 3.5. For comparison, the ratio of SOCvoc/CO was also estimated from the emissions inventory of VOCs and CO in Shanghai. The CO emissions inventory in 2013 was used as the average of data from the MEIC in 2012 and 2014 developed by Tsinghua University (http://www.meicmodel.

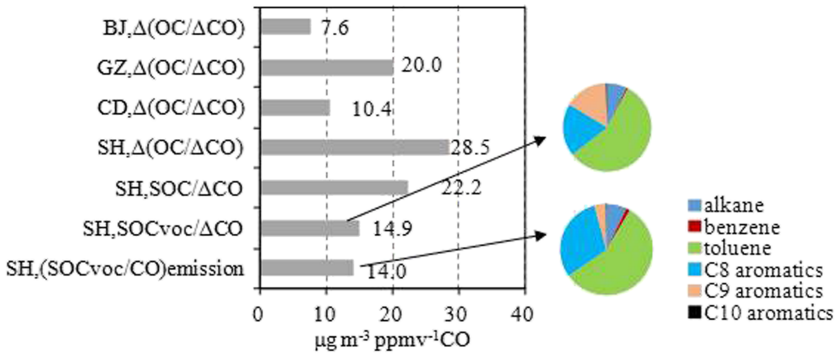


**Figure 9.** Comparisons of SOC formation in eastern China obtained by different methods. SOC formation in Shanghai (SH, the bottom four columns) based on the VOC emissions inventory (SH, $(SOCvoc/CO)_{emission}$) and VOC measurements in the ambient environment (SH, SOCvoc/CO), total SOC (SH, SOC/ΔCO) estimated by the parameterization method and the increase of the ratio of OC/ΔCO (SH, Δ (OC/ΔCO)) in this study were presented. The contributions of VOC species to SOC formation in Shanghai were shown in color in pie charts. SOC formation in Changdao was indicated by the increase in the ratio of OC/ΔCO (CD, Δ (OC/ΔCO)) (Yuan et al., *2013*). SOC formation in Beijing and Guangzhou were indicated by the increase in the ratio of OC/ΔCO (GZ, Δ (OC/ΔCO)) (Hu et al., *2012;* Hu et al., *2017*).

org/). The speciated VOC emissions inventory in 2013 was obtained from Wu and Xie (2017), and for comparison, only emissions of VOC species measured in the present study were considered. Thus, the ratio of $(SOCvoc/CO)_{emission}$ could be calculated from the product of the emission ratios of VOCs to CO, the SOA yields of VOCs under high $NO_x$ levels, and the proportions of VOC photochemical consumption. The proportions of VOC photochemical consumption to total VOC emissions were calculated with the assumption that VOC emissions had the same OH exposure ($\Delta t$[OH], as shown in equation 2) as the measured VOCs during the pollution episode. Accordingly, the ratio of $(SOCvoc/CO)_{emission}$ was estimated to be 14.0 $\mu g\ m^{-3}\ ppmv^{-1}$, being comparable with the observation-based ratio of SOCvoc/CO. However, there were some differences in VOC species contributing to SOC formation between the ambient observation-based result and the emission-based result, as shown in Figure 9. Compared with the observation-based result, the contribution of C9 aromatics to SOC formation was severely underestimated in the emission-based result, and correspondingly the contribution of other VOC species, mainly C8 aromatics, was overestimated. These results suggest that bias might exist in the VOC source profiles in the previous VOC emissions inventory.

## 4. Conclusions

An episode of heavy photochemical smog was observed in the summer of 2013 in Shanghai, China. During this episode, $O_3$ and OC in $PM_{2.5}$ increased simultaneously and the VOCs diurnal pattern was completely opposite to those displayed by $O_3$ and OC. The photochemical processing of VOCs and OC was studied by a parameterization method. VOC photochemical consumption was estimated and found to differ substantially from the ambient measured VOCs both in terms of the diurnal pattern and the species compositions. More than half of the VOCs consumed were aromatics which also dominated (93%) the SOC formation from VOCs. SOC formation from VOCs was estimated to be $3.9 \pm 1.0\ \mu g/m^3$, explaining about 67% of the total SOC ($5.8 \pm 3.6\ \mu g/m^3$) as derived by the parameterization method and further confirmed by the EC tracer method.

According to the OC evolution, the emission ratio of OC to CO was estimated to be $5.8 \pm 0.5\ \mu g\ m^{-3}\ ppmv^{-1}$, lower than the emissions inventory value of ~8 $\mu g\ m^{-3}\ ppmv^{-1}$ in Shanghai. Moreover, the ratio of SOC to ΔCO (SOC/ΔCO) was found to be $22.2 \pm 5.7\ \mu g\ m^{-3}\ ppmv^{-1}$, among which 66.9% came from SOC formation from VOC photochemical processing (SOCvoc/ΔCO). For comparison, the ratio of SOC to CO was also calculated based on the emissions inventory of speciated VOCs and CO ($(SOCvoc/CO)_{emission}$), assuming that VOC emissions had the same OH exposure as the VOCs measured during the present episode. It turned out that $(SOCvoc/CO)_{emission}$ was 14.0 $\mu g\ m^{-3}\ ppmv^{-1}$ and comparable with the ambient SOCvoc/ΔCO, while the precursor compositions were very different. This suggests that there might be a large bias in the VOC source profiles of the emissions inventory.

The present study highlights the importance of the oxidation of VOCs, especially aromatics, for the formation of SOC during photochemical pollution episode in Shanghai. The study also reveals that a large bias likely exists in the species compositions in the emissions inventory. It is essential to improve the VOC emissions inventory, which is critical for making policies and formulating strategies to control air pollution.

**Acknowledgments**
This work was supported by the National Key R&D Program of China (2018YFC0213801), the National Natural Science Foundation of China (21607104), the Shanghai Science and Technology Commission of the Shanghai Municipality (18QA1403600), and the Shanghai Environmental Protection Bureau (2017-2). The data in the present study could be downloaded via doi: 10.17632/jtp5tck2g9.1 (Wang, 20202020).

## References

Ait-Helal, W., Borbon, A., Sauvage, S., de Gouw, J. A., Colomb, A., Gros, V., et al. (2014). Volatile and intermediate volatility organic compounds in suburban Paris: Variability, origin and importance for SOA formation. *Atmospheric Chemistry and Physics*, *14*(19), 10,439–10,464. https://doi.org/10.5194/acp-14-10439-2014

An, Z., Huang, R. J., Zhang, R., Tie, X., Li, G., Cao, J., et al. (2019). Severe haze in northern China: A synergy of anthropogenic emissions and atmospheric processes. *Proceedings of the National Academy of Sciences of the United States of America*, *116*(18), 8657–8666. https://doi.org/10.1073/pnas.1900125116

Atkinson, R., Baulch, D. L., Cox, R. A., Crowley, J. N., Hampson, R. F., Hynes, R. G., et al. (2006). Evaluated kinetic and photochemical data for atmospheric chemistry: Volume II—Gas phase reactions of organic species. *Atmospheric Chemistry and Physics*, *6*, 3625–4055.

Cao, J. J., Lee, S. C., Chow, J. C., Watson, J. G., Ho, K. F., Zhang, R. J., et al. (2007). Spatial and seasonal distributions of carbonaceous aerosols over China. *Journal of Geophysical Research*, *112*, D22S11. https://doi.org/10.1029/2006jd008205

Chan, A. W. H., Kautzman, K. E., Chhabra, P. S., Surratt, J. D., Chan, M. N., Crounse, J. D., et al. (2009). Secondary organic aerosol formation from photooxidation of naphthalene and alkylnaphthalenes: Implications for oxidation of intermediate volatility organic compounds (IVOCs). *Atmospheric Chemistry and Physics*, *9*, 3049–3060.

Claeys, M., Graham, B., Vas, G., Wang, W., Vermeylen, R., Pashynska, V., et al. (2004). Formation of secondary organic aerosols through photooxidation of isoprene. *Science*, *303*(5661), 1173–1176. https://doi.org/10.1126/science.1092805

de Gouw, J. A. (2005). Budget of organic carbon in a polluted atmosphere: Results from the New England Air Quality Study in 2002. *Journal of Geophysical Research*, *110*, D16305. https://doi.org/10.1029/2004jd005623

de Gouw, J. A., Brock, C. A., Atlas, E. L., Bates, T. S., Fehsenfeld, F. C., Goldan, P. D., et al. (2008). Sources of particulate matter in the northeastern United States in summer: 1. Direct emissions and secondary formation of organic matter in urban plumes. *Journal of Geophysical Research*, *113*, D08301. https://doi.org/10.1029/2007jd009243

DeCarlo, P. F., Ulbrich, I. M., Crounse, J., de Foy, B., Dunlea, E. J., Aiken, A. C., et al. (2010). Investigation of the sources and processing of organic aerosol over the Central Mexican Plateau from aircraft measurements during MILAGRO. *Atmospheric Chemistry and Physics*, *10*, 5257–5280. https://doi.org/10.5194/acp-10-5257-2010

Ding, A. J., Fu, C. B., Yang, X. Q., Sun, J. N., Zheng, L. F., Xie, Y. N., et al. (2013). Ozone and fine particle in the western Yangtze River Delta: An overview of 1 yr data at the SORPES station. *Atmospheric Chemistry and Physics*, *13*(11), 5813–5830. https://doi.org/10.5194/acp-13-5813-2013

Ding, X., Wang, X.-M., Gao, B., Fu, X.-X., He, Q.-F., Zhao, X.-Y., et al. (2012). Tracer-based estimation of secondary organic carbon in the Pearl River Delta, south China. *Journal of Geophysical Research*, *117*, D05313. https://doi.org/10.1029/2011jd016596

Ehhalt, D. H., & Rohrer, F. (2000). Dependence of the OH concentration on solar UV. *Journal of Geophysical Research*, *105*, 3565–3571.

Ehn, M., Thornton, J. A., Kleist, E., Sipilä, M., Junninen, H., Pullinen, I., et al. (2014). A large source of low-volatility secondary organic aerosol. *Nature*, *506*(7489), 476–479. https://doi.org/10.1038/nature13032

Emanuelsson, E. U., Hallquist, M., Kristensen, K., Glasius, M., Bohn, B., Fuchs, H., et al. (2013). Formation of anthropogenic secondary organic aerosol (SOA) and its influence on biogenic SOA properties. *Atmospheric Chemistry and Physics*, *13*(5), 2837–2855. https://doi.org/10.5194/acp-13-2837-2013

Feng, T., Zhao, S., Bei, N., Wu, J., Liu, S., Li, X., et al. (2019). Secondary organic aerosol enhanced by increasing atmospheric oxidizing capacity in Beijing–Tianjin–Hebei (BTH), China. *Atmospheric Chemistry and Physics*, *19*(11), 7429–7443. https://doi.org/10.5194/acp-19-7429-2019

Fu, X., Wang, S., Zhao, B., Xing, J., Cheng, Z., Liu, H., & Hao, J. (2013). Emission inventory of primary pollutants and chemical speciation in 2010 for the Yangtze River Delta region, China. *Atmospheric Environment*, *70*, 39–50. https://doi.org/10.1016/j.atmosenv.2012.12.034

Gao, Y., Wang, H., Zhang, X., Jing, S., Peng, Y., Qiao, L., et al. (2019). Estimating secondary organic aerosol production from toluene photochemistry in a megacity of China. *Environmental Science & Technology*, *53*(15), 8664–8671. https://doi.org/10.1021/acs.est.9b00651

Guo, S., Hu, M., Guo, Q., & Shang, D. (2014). Comparison of secondary organic aerosol estimation methods. *Acta Chimica Sinica*, *72*(6), 658. https://doi.org/10.6023/a14040254

Guo, S., Hu, M., Guo, Q., Zhang, X., Schauer, J. J., & Zhang, R. (2013). Quantitative evaluation of emission controls on primary and secondary organic aerosol sources during Beijing 2008 Olympics. *Atmospheric Chemistry and Physics*, *13*(16), 8303–8314. https://doi.org/10.5194/acp-13-8303-2013

Guo, S., Hu, M., Guo, Q. F., Zhang, X., Zheng, M., Zheng, J., et al. (2012). Primary sources and secondary formation of organic aerosols in Beijing, China. *Environmental Science & Technology*, *46*(18), 9846–9853. https://doi.org/10.1021/Es20425641

Guo, S., Hu, M., Peng, J., Wu, Z., Zamora, M. L., Shang, D., et al. (2020). Remarkable nucleation and growth of ultrafine particles from vehicular exhaust. *Proceedings of the National Academy of Sciences*, *117*(7), 3427–3432. https://doi.org/10.1073/pnas.1916366117

Hayes, P. L., Carlton, A. G., Baker, K. R., Ahmadov, R., Washenfelder, R. A., Alvarez, S., et al. (2015). Modeling the formation and aging of secondary organic aerosols in Los Angeles during CalNex 2010. *Atmospheric Chemistry and Physics*, *15*(10), 5773–5801. https://doi.org/10.5194/acp-15-5773-2015

Hayes, P. L., Ortega, A. M., Cubison, M. J., Froyd, K. D., Zhao, Y., Cliff, S. S., et al. (2013). Organic aerosol composition and sources in Pasadena, California, during the 2010 CalNex campaign. *Journal of Geophysical Research: Atmospheres*, *118*, 9233–9257. https://doi.org/10.1002/jgrd.50530

Heo, J., de Foy, B., Olson, M. R., Pakbin, P., Sioutas, C., & Schauer, J. J. (2015). Impact of regional transport on the anthropogenic and biogenic secondary organic aerosols in the Los Angeles Basin. *Atmospheric Environment*, *103*, 171–179. https://doi.org/10.1016/j.atmosenv.2014.12.041

Hoyle, C. R., Myhre, G., Berntsen, T. K., & Isaksen, I. S. A. (2009). Anthropogenic influence on SOA and the resulting radiative forcing. *Atmospheric Chemistry and Physics*, *9*, 2715–2728.

Hu, W., Hu, M., Hu, W.-W., Zheng, J., Chen, C., Wu, Y., & Guo, S. (2017). Seasonal variations in high time-resolved chemical compositions, sources, and evolution of atmospheric submicron aerosols in the megacity Beijing. *Atmospheric Chemistry and Physics*, *17*(16), 9979–10,000. https://doi.org/10.5194/acp-17-9979-2017

Hu, W. W., Hu, M., Deng, Z. Q., Xiao, R., Kondo, Y., Takegawa, N., et al. (2012). The characteristics and origins of carbonaceous aerosol at a rural site of PRD in summer of 2006. *Atmospheric Chemistry and Physics*, *12*(4), 1811–1822. https://doi.org/10.5194/acp-12-1811-2012

Hu, W. W., Hu, M., Yuan, B., Jimenez, J. L., Tang, Q., Peng, J. F., et al. (2013). Insights on organic aerosol aging and the influence of coal combustion at a regional receptor site of central eastern China. *Atmospheric Chemistry and Physics*, *13*(19), 10,095–10,112. https://doi.org/10.5194/acp-13-10095-2013

Huang, R. J., Zhang, Y., Bozzetti, C., Ho, K. F., Cao, J. J., Han, Y., et al. (2014). High secondary aerosol contribution to particulate pollution during haze events in China. *Nature*, *514*(7521), 218–222. https://doi.org/10.1038/nature13774

Huang, X. F., He, L. Y., Xue, L., Sun, T. L., Zeng, L. W., Gong, Z. H., et al. (2012). Highly time-resolved chemical characterization of atmospheric fine particles during 2010 Shanghai World Expo. *Atmospheric Chemistry and Physics*, *12*(11), 4897–4907. https://doi.org/10.5194/acp-12-4897-2012

Jang, M., Czoschke, N. M., Lee, S., & Kamens, R. M. (2002). Heterogeneous atmospheric aerosol production by acid-catalyzed particle-phase reactions. *Science*, *298*(5594), 814–817. https://doi.org/10.1126/science.1075798

Jimenez, J. L., Canagaratna, M. R., Donahue, N. M., Prevot, A. S., Zhang, Q., Kroll, J. H., et al. (2009). Evolution of organic aerosols in the atmosphere. *Science*, *326*(5959), 1525–1529. https://doi.org/10.1126/science.1180353

Kanakidou, M., Seinfeld, J. H., Pandis, S. N., Barnes, I., Dentener, F. J., Facchini, M. C., et al. (2005). Organic aerosol and global climate modeling: A review. *Atmospheric Chemistry and Physics*, *5*, 1053–1123.

Kleindienst, T. E., Jaoui, M., Lewandowski, M., Offenberg, J. H., Lewis, C. W., Bhave, P. V., & Edney, E. O. (2007). Estimates of the contributions of biogenic and anthropogenic hydrocarbons to secondary organic aerosol at a southeastern US location. *Atmospheric Environment*, *41*(37), 8288–8300. https://doi.org/10.1016/j.atmosenv.2007.06.045

Kleinman, L., Kuang, C., Sedlacek, A., Senum, G., Springston, S., Wang, J., et al. (2016). What do correlations tell us about anthropogenic–biogenic interactions and SOA formation in the Sacramento plume during CARES? *Atmospheric Chemistry and Physics*, *16*(3), 1729–1746. https://doi.org/10.5194/acp-16-1729-2016

Koch, D. (2001). Transport and direct radiative forcing of carbonaceous and sulfate aerosols in the GISS GCM. *Journal of Geophysical Research*, *106*, 20,311–20,332.

Koss, A. R., de Gouw, J., Warneke, C., Gilman, J. B., Lerner, B. M., Graus, M., et al. (2015). Photochemical aging of volatile organic compounds associated with oil and natural gas extraction in the Uintah Basin, UT, during a wintertime ozone formation event. *Atmospheric Chemistry and Physics*, *15*(10), 5727–5741. https://doi.org/10.5194/acp-15-5727-2015

Li, K., Jacob, D. J., Liao, H., Shen, L., Zhang, Q., & Bates, K. H. (2019). Anthropogenic drivers of 2013-2017 trends in summer surface ozone in China. *Proceedings of the National Academy of Sciences of the United States of America*, *116*(2), 422–427. https://doi.org/10.1073/pnas.1812168116

Li, M., Zhang, Q., Kurokawa, J.-I., Woo, J.-H., He, K., Lu, Z., et al. (2017). MIX: A mosaic Asian anthropogenic emission inventory under the international collaboration framework of the MICS-Asia and HTAP. *Atmospheric Chemistry and Physics*, *17*, 935–963. https://doi.org/10.5194/acp-17-935-2017

Li, M., Zhang, Q., Streets, D. G., He, K. B., Cheng, Y. F., Emmons, L. K., et al. (2014). Mapping Asian anthropogenic emissions of non-methane volatile organic compounds to multiple chemical mechanisms. *Atmospheric Chemistry and Physics*, *14*(11), 5617–5638. https://doi.org/10.5194/acp-14-5617-2014

Li, Y. J., Lee, B. P., Su, L., Fung, J. C. H., & Chan, C. K. (2015). Seasonal characteristics of fine particulate matter (PM) based on high-resolution time-of-flight aerosol mass spectrometric (HR-ToF-AMS) measurements at the HKUST supersite in Hong Kong. *Atmospheric Chemistry and Physics*, *15*(1), 37–53. https://doi.org/10.5194/acp-15-37-2015

Lim, Y. B., & Ziemann, P. J. (2009). Effects of molecular structure on aerosol yields from OH radical-initiated reactions of linear, branched, and cyclic alkanes in the presence of $NO_x$. *Environmental Science & Technology*, *43*(7), 2328–2334. https://doi.org/10.1021/es803389s

Liu, P., Li, Y. J., Wang, Y., Gilles, M. K., Zaveri, R. A., Bertram, A. K., & Martin, S. T. (2016). Lability of secondary organic particulate matter. *Proceedings of the National Academy of Sciences of the United States of America*, *113*(45), 12,643–12,648. https://doi.org/10.1073/pnas.1603138113

Liu, Y., Wang, H., Jing, S., Gao, Y., Peng, Y., Lou, S., et al. (2019). Characteristics and sources of volatile organic compounds (VOCs) in Shanghai during summer: Implications of regional transport. *Atmospheric Environment*, *215*, 116902. https://doi.org/10.1016/j.atmosenv.2019.116902

Millet, D. B., Goldstein, A. H., Allan, J. D., Bates, T. S., Boudries, H., Bower, K. N., et al. (2004). Volatile organic compound measurements at Trinidad Head, California, during ITCT 2K2: Analysis of sources, atmospheric composition, and aerosol residence times. *Journal of Geophysical Research*, *109*, D23S16. https://doi.org/10.1029/2003JD004026

Ng, N. L., Kroll, J. H., Chan, A. W. H., Chhabra, P. S., Flagan, R. C., & Seinfeld, J. H. (2007). Secondary organic aerosol formation from m-xylene, toluene, and benzene. *Atmospheric Chemistry and Physics*, *7*, 3909–3922.

Odum, J. R., Hoffmann, T., Bowman, F., Collins, D., Flagan, R. C., & Seinfeld, J. H. (1996). Gas/particle partitioning and secondary organic aerosol yields. *Environmental Science & Technology*, *30*, 2580–2585.

Palm, B. B., de Sá, S. S., Day, D. A., Campuzano-Jost, P., Hu, W., Seco, R., et al. (2018). Secondary organic aerosol formation from ambient air in an oxidation flow reactor in Central Amazonia. *Atmospheric Chemistry and Physics*, *18*(1), 467–493. https://doi.org/10.5194/acp-18-467-2018

Praske, E., Otkjær, R. V., Crounse, J. D., Hethcox, J. C., Stoltz, B. M., Kjaergaard, H. G., & Wennberg, P. O. (2018). Atmospheric autoxidation is increasingly important in urban and suburban North America. *Proceedings of the National Academy of Sciences of the United States of America*, *115*(1), 64–69. https://doi.org/10.1073/pnas.1715540115

Qiao, L., Cai, J., Wang, H., Wang, W., Zhou, M., Lou, S., et al. (2014). $PM_{2.5}$ constituents and hospital emergency-room visits in Shanghai, China. *Environmental Science & Technology*, *48*(17), 10,406–10,414. https://doi.org/10.1021/es501305k

Robinson, A. L., Donahue, N. M., Shrivastava, M. K., Weitkamp, E. A., Sage, A. M., Grieshop, A. P., et al. (2007). Rethinking organic aerosols: Semivolatile emissions and photochemical aging. *Science*, *315*(5816), 1259–1262. https://doi.org/10.1126/science.1133061

Schwantes, R. H., Schilling, K. A., McVay, R. C., Lignell, H., Coggon, M. M., Zhang, X., et al. (2017). Formation of highly oxygenated low-volatility products from cresol oxidation. *Atmospheric Chemistry and Physics*, *17*(5), 3453–3474. https://doi.org/10.5194/acp-17-3453-2017

Seinfeld, J. H., & Pandis, S. N. (2006). *Atmospheric chemistry and physics: From air pollution to climate change*, (p. 1203). New York: Wiley, John & Sons, Incorporated.

Shrivastava, M., Cappa, C. D., Fan, J., Goldstein, A. H., Guenther, A. B., Jimenez, J. L., et al. (2017). Recent advances in understanding secondary organic aerosol: Implications for global climate forcing. *Reviews of Geophysics*, *55*, 509–559. https://doi.org/10.1002/2016RG000540

Sjostedt, S. J., Slowik, J. G., Brook, J. R., Chang, R. Y. W., Mihele, C., Stroud, C. A., et al. (2011). Diurnally resolved particulate and VOC measurements at a rural site: Indication of significant biogenic secondary organic aerosol formation. *Atmospheric Chemistry and Physics*, *11*(12), 5745–5760. https://doi.org/10.5194/acp-11-5745-2011

Slowik, J. G. (2010). Simultaneous factor analysis of organic particle and gas mass spectra: AMS and PTR-MS measurements at an urban site. *Atmospheric Chemistry and Physics*, *10*(4).

Spracklen, D. V., Jimenez, J. L., Carslaw, K. S., Worsnop, D. R., Evans, M. J., Mann, G. W., et al. (2011). Aerosol mass spectrometer constraint on the global secondary organic aerosol budget. *Atmospheric Chemistry and Physics*, *11*, 12,109–12,136.

Sun, Y., Wang, Z., Fu, P., Jiang, Q., Yang, T., Li, J., & Ge, X. (2013). The impact of relative humidity on aerosol composition and evolution processes during wintertime in Beijing, China. *Atmospheric Environment*, *77*, 927–934. https://doi.org/10.1016/j.atmosenv.2013.06.019

Tan, Z., Lu, K., Jiang, M., Su, R., Wang, H., Lou, S., et al. (2019). Daytime atmospheric oxidation capacity in four Chinese megacities during the photochemically polluted season: A case study based on box model simulation. *Atmospheric Chemistry and Physics*, *19*(6), 3493–3513. https://doi.org/10.5194/acp-19-3493-2019

Turpin, B. J., & Huntzicker, J. J. (1995). Identification of secondary organic aerosol episodes and quantitation of primary and secondary organic aerosol concentrations during Scaqs. *Atmospheric Environment*, *29*(23), 3527–3544.

Volkamer, R., Jimenez, J. L., San Martini, F., Dzepina, K., Zhang, Q., Salcedo, D., et al. (2006). Secondary organic aerosol formation from anthropogenic air pollution: Rapid and higher than expected. *Geophysical Research Letters*, *33*, L17811. https://doi.org/10.1029/2006gl026899

Wang, H. L., Chen, C. H., Wang, Q., Huang, C., Su, L. Y., Huang, H. Y., et al. (2013). Chemical loss of volatile organic compounds and its impact on the source analysis through a two-year continuous measurement. *Atmospheric Environment*, *80*, 488–498.

Wang, H. L., Qiao, L. P., Lou, S. R., Zhou, M., Chen, J. M., Wang, Q., et al. (2015). $PM_{2.5}$ pollution episode and its contributors from 2011 to 2013 in urban Shanghai, China. *Atmospheric Environment*, *123*, 298–305. https://doi.org/10.1016/j.atmosenv.2015.08.018

Wang, H. L., Qiao, L. P., Lou, S. R., Zhou, M., Ding, A. J., Huang, H. Y., et al. (2016). Chemical composition of $PM_{2.5}$ and meteorological impact among three years in urban Shanghai, China. *Journal of Cleaner Production*, *112*, 1302–1311. https://doi.org/10.1016/j.jclepro.2015.04.099

Wang, Hongli (2020), "Estimation of secondary organic aerosol formation during a photochemical smog episode in Shanghai, China-data", Mendeley Data, v1.

Weber, R. J., Sullivan, A. P., Peltier, R. E., Russell, A., Yan, B., Zheng, M., et al. (2007). A study of secondary organic aerosol formation in the anthropogenic-influenced southeastern United States. *Journal of Geophysical Research*, *112*, D13302. https://doi.org/10.1029/2007jd008408

Wu, R., & Xie, S. (2017). Spatial distribution of ozone formation in China derived from emissions of speciated volatile organic compounds. *Environmental Science & Technology*, *51*(5), 2574–2583. https://doi.org/10.1021/acs.est.6b03634

Xu, W., Han, T., du, W., Wang, Q., Chen, C., Zhao, J., et al. (2017). Effects of aqueous-phase and photochemical processing on secondary organic aerosol formation and evolution in Beijing, China. *Environmental Science & Technology*, *51*(2), 762–770. https://doi.org/10.1021/acs.est.6b04498

Yuan, B., Hu, W. W., Shao, M., Wang, M., Chen, W. T., Lu, S. H., et al. (2013). VOC emissions, evolutions and contributions to SOA formation at a receptor site in eastern China. *Atmospheric Chemistry and Physics*, *13*(17), 8815–8832. https://doi.org/10.5194/acp-13-8815-2013

Yuan, Z. B., Yu, J. Z., Lau, A. K. H., Louie, P. K. K., & Fung, J. C. H. (2006). Application of positive matrix factorization in estimating aerosol secondary organic carbon in Hong Kong and its relationship with secondary sulfate. *Atmospheric Chemistry and Physics*, *6*, 25–34.

Zhang, Q. (2005). Time- and size-resolved chemical composition of submicron particles in Pittsburgh: Implications for aerosol sources and processes. *Journal of Geophysical Research*, *110*, D07S09. https://doi.org/10.1029/2004jd004649

Zhang, X., Cappa, C. D., Jathar, S. H., McVay, R. C., Ensberg, J. J., Kleeman, M. J., & Seinfeld, J. H. (2014). Influence of vapor wall loss in laboratory chambers on yields of secondary organic aerosol. *Proceedings of the National Academy of Sciences of the United States of America*, *111*, 5802–5807. https://doi.org/10.1073/pnas.1404727111

Zhang, X. Y., Wang, Y. Q., Zhang, X. C., Guo, W., & Gong, S. L. (2008). Carbonaceous aerosol composition over various regions of China during 2006. *Journal of Geophysical Research*, *113*, D14111. https://doi.org/10.1029/2007JD009525

Zheng, M., Cass, G. R., Schauer, J. J., & Edgerton, E. S. (2002). Source apportionment of $PM_{2.5}$ in the southeastern United States using solvent extractable organic compounds as tracers. *Environmental Science & Technology*, *36*(11), 2361–2371. https://doi.org/10.1021/es011275x

Zhou, W., Cohan, D. S., & Henderson, B. H. (2014). Slower ozone production in Houston, Texas following emission reductions: Evidence from Texas air quality studies in 2000 and 2006. *Atmospheric Chemistry and Physics*, *14*(6), 2777–2788. https://doi.org/10.5194/acp-14-2777-2014